CrystEngComm

PAPER

View Article Online
View Journal | View Issue

The atomic origin of high catalytic activity of ZnO nanotetrapods for decomposition of ammonium perchlorate†

Cite this: *CrystEngComm*, 2014, **16**, 570

Gen Tang,‡[ac] Yanwei Wen,‡[ab] Aiming Pang,[c] Dawen Zeng,*[ab] Yungang Zhang,[ac] Shouqin Tian,[ad] Bin Shan*[ab] and Changsheng Xie[b]

Received 19th July 2013,
Accepted 14th November 2013

DOI: 10.1039/c3ce41435c

www.rsc.org/crystengcomm

Distinct from the common well faceted ZnO nanorods (R-ZnO), ZnO nanotetrapods (T-ZnO) exhibited a remarkable catalytic activity for the thermal decomposition of ammonium perchlorate (AP): the activation energy at high temperature decomposition (HTD) was significantly decreased to 111.9 kJ mol^{-1}, much lower than 162.5 kJ mol^{-1} for pure AP and 156.9 kJ mol^{-1} for AP with R-ZnO. This was attributed to more abundant atomic steps on the surface of T-ZnO than that of R-ZnO, as evidenced by HRTEM and density function theory (DFT) calculations. It was shown that the initiation step of perchloric acid (PA) decomposition happened much faster on stepped T-ZnO edges, resulting in the formation of active oxygen atoms from $HClO_4$. The formed oxygen atoms would subsequently react with NH_3 to produce HNO, N_2O and NO species, thus leading to an obvious decrease in the activation energy of AP decomposition. The proposed catalytic mechanism was further corroborated by the TG-IR spectroscopy results. Our work can provide atomic insights into the catalytic decomposition of AP on ZnO nanostructures.

It is well known that AP is one of the most common oxidants in composite solid propellants and pyrotechnics, which operate at high temperatures and stresses in general.[1] The thermal decomposition rate of AP is closely related to the additives, which can greatly influence the burning rate and pressure exponent of the propellant.[2] A specific feature of AP decomposition is its extremely high sensitivity to the action of various additives.[3] This has stimulated much attention from many researchers, especially those dealing with the development of solid propellants.[4,5] Many studies have been carried out to lower the thermal decomposition temperature of AP and to increase the heat release by developing different catalysts, such as transition metals,[6–13] rare earth metals,[14–16] and their compounds[17–19] in the past decades. ZnO, as one of the best single metal oxide catalysts, is used indispensably in the chemical industry and the photochemical industry, owing to its excellent reactivity, non-toxicity and stability.[20] Recently, ZnO twin-cones,[21] nitrogen-doped ZnO nanocrystallites[22] and ZnO nanorod-assembled hollow superstructures[23] have been explored as catalysts to promote the thermal decomposition of AP. To explain the decomposition mechanism of AP with ZnO additives, two assumptions have been proposed. The first one is the formation of easily melting eutectics between oxide additives and AP, due to the transition from the solid state into liquid.[24] The other assumption is attributed to V_O-related defects and the release of oxygen.[21] However, the two assumptions lack solid and direct evidence, and thus it is difficult to further reveal the catalytic mechanism of ZnO for AP decomposition, especially at the atomic or molecular level. This is because the surface atomic structure of ZnO nanocrystals will probably play a very important role in the catalytic decomposition of AP. Therefore, it is of great significance to understand the catalytic mechanism of ZnO in the decomposition of AP from atomic insights.

We report here the excellent catalytic activity of T-ZnO towards the thermal decomposition of AP due to the unique stepped configurations of T-ZnO, which are characterized using the HRTEM technique. With a few surface atomic steps, well faceted R-ZnO exhibit an inferior catalytic activity. Interestingly, active oxygen atoms on the steps of T-ZnO are the key to highly efficient thermal decomposition as revealed by density-functional theory (DFT) calculations and confirmed by IR spectroscopy. In addition, the reaction pathway reveals that the unique atomic step configurations could

[a] *State Key Laboratory of Materials Processing and Die & Mould Technology, Huazhong University of Science and Technology (HUST), No. 1037, Luoyu Road, Wuhan 430074, PR China. E-mail: dwzeng@mail.hust.edu.cn; Fax: +86 027 87543778; Tel: +86 027 87559835*
[b] *Department of Materials Science and Engineering, HUST, No. 1037, Luoyu Road, Wuhan 430074, PR China. E-mail: bshan@mail.hust.edu.cn*
[c] *Hubei Institute of Aerospace Chemotechnology, No. 58, Qinghe Road, Xiangyang 441003, PR China*
[d] *State Key Laboratory of Silicate Materials for Architectures, Wuhan University of Technology, No. 122, Luoshi Road, Wuhan 430070, PR China*

† Electronic supplementary information (ESI) available. See DOI: 10.1039/c3ce41435c

‡ Gen Tang and Yanwei Wen contributed equally to this work.

facilitate the initiation of the combustion process, *i.e.* formation of active oxygen atoms from $HClO_4$. The formed active oxygen atoms can react with NH_3 to produce HNO and N_2O species, thus leading to a significant decrease in the activation energy of AP decomposition. Our investigation offers new insights into the interaction between AP and T-ZnO, and the mechanism of ZnO-involved heterogeneous catalytic reactions.

Fig. 1 shows the experimentally measured values of $\ln(\beta/T_p^2)$ *versus* $1/T_p$ for AP decomposition with ZnO additives, which are calculated from the exothermic peak temperature dependence on the heating rate as described using the Kissinger correlation ($\ln(\beta/T_p^2) = \ln(AR/E_a^2) - E_a/RT_p$). In this formula, β is the heating rate in degrees Celsius per minute, T_p is the peak temperature, R is the ideal gas constant, A is the pre-exponential factor and E_a is the activation energy. Also, Table 1 summarizes the kinetic parameters of pure AP, AP with T-ZnO and R-ZnO in low-temperature decomposition (LTD) and high-temperature decomposition (HTD) processes. The calculation details are described as shown in S-III.† For pure AP, the activation energy E_a of LTD and HTD is calculated to be 137.2 ± 1.6 and 162.5 ± 7.6 kJ mol^{-1}, respectively, which are close to the values previously reported in the literature.[22] In the presence of T-ZnO, the activation energy E_a of AP decomposition is decreased significantly to 109.9 ± 2.3 kJ mol^{-1} for LTD and 111.9 ± 6.9 kJ mol^{-1} for HTD while R-ZnO as additives lower the activation energy to 117.9 ± 6.6 kJ mol^{-1} for LTD and 156.9 ± 15.1 kJ mol^{-1} for HTD. It can be seen that T-ZnO and R-ZnO exhibit an obvious catalytic activity for AP decomposition. Moreover, the catalytic activity of T-ZnO is better than that of R-ZnO, probably because of the difference in their surface atomic structure.

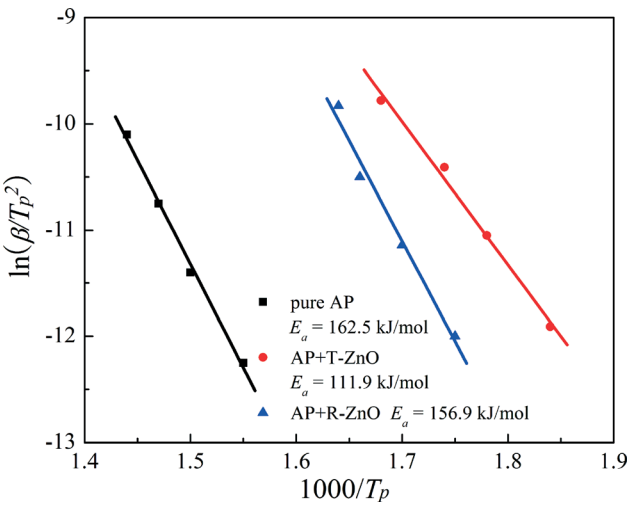

Fig. 1 Dependence of $\ln(\beta/T_p^2)$ on $1/T_p$ for AP and mixtures of AP with ZnO additives in the HTD stage. Scatter points are experimental data and lines denote the linear fitting results.

Table 1 Kinetic parameters of pure AP and AP with ZnO additives in LTD and HTD processes

	LTD		HTD	
Sample	E_a (kJ mol^{-1})	R^2	E_a (kJ mol^{-1})	R^2
AP	137.2 ± 1.6	0.9998	162.5 ± 7.6	0.9978
AP + T-ZnO	109.9 ± 2.3	0.9995	111.9 ± 6.9	0.9962
AP + R-ZnO	117.9 ± 6.6	0.9969	156.9 ± 15.1	0.9909

As known, the properties of materials depend deeply on their structures, especially surface atomic structures. The phase structure of T-ZnO and R-ZnO was characterized using XRD. Their corresponding XRD patterns are shown in Fig. S1.† It is found that T-ZnO and R-ZnO belong to hexagonal wurtzite structured ZnO with lattice parameters a = 0.3249 nm and c = 0.5206 nm (JCPDS card, no. 36-1451). TEM and HRTEM were also employed to characterize T-ZnO and R-ZnO, and the corresponding images are presented in Fig. 2. For T-ZnO, each particle consists of four feet with a length of up to 200 nm (called T-ZnO) as shown in Fig. 2(a). The diameter of every foot is gradually decreased from the cross (~40 nm) to the foot tip (~20 nm). Thus, the average diameter is considered to be ~30 nm and the specific surface area of T-ZnO is only 4.5 m^2 g^{-1} in our previous report.[25] Upon decreasing the diameter, some surfaces with concave curvatures appear on the side face of the foot (Fig. 2(b)). On these surfaces, there are abundant atomic steps that consist of exposed {10–10} and (0001) facets in the HRTEM images in Fig. 2(c–d), in which the lattice spacing of 0.51 nm and 0.28 nm between the adjacent lattice planes corresponds to the d-spacing of (0001) planes and {10–10} facets,[26] respectively. It can be seen that these steps appear on the whole side face of every foot. In addition, exposed faces with Miller indices of (0001) and {10–10} can also be frequently observed on the surface of a foot tip as shown in Fig. 2(e). For the surface with convex curvatures, a relatively high density of atomic steps and kinks can also be expected. As a comparison, R-ZnO exhibits a diameter of ~50 nm and length of up to ~400 nm as shown in Fig. 2(f–h). The surface/volume ratio can be calculated as 0.085 m^2 m^{-3} but the specific surface area of such nanorods was reported to be 4–8 m^2 g^{-1} in other similar studies.[27,28] In this sense, the diameter and length of R-ZnO are slightly larger than that of T-ZnO, but both samples have a similar specific surface area. In addition, R-ZnO show very well-faceted crystals, and their

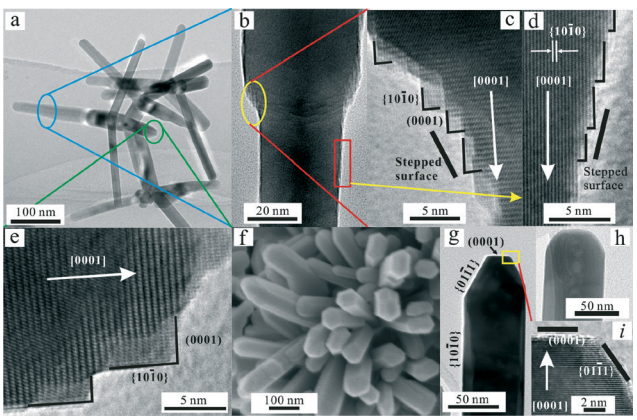

Fig. 2 (a) TEM and (b–e) HRTEM images of T-ZnO including stepped surfaces; (f) FSEM and (g–i) TEM images of R-ZnO.

side faces have exposed {10–10} facets and are very flat (Fig. 2(g–h)), in good agreement with a previous work.[29] Near the end face, there is an exposed {01–11} facet (Fig. 2(g) and (i)) or the convex curvature (Fig. 2(h)) connected with side surface {10–10} facets and an end face (0001) plane. There are only a few kinks or steps at the connection, indicating a lower density of the stepped surfaces on R-ZnO than that on T-ZnO. Therefore, the great difference between T-ZnO and R-ZnO is mainly shown in the surface structure rather than in the size and specific surface area, which can explain the above distinct catalytic performance.

To further investigate the role of T-ZnO's atomic steps in the catalytic decomposition of AP, DFT calculations and the nudged elastic band method (NEB) were employed. The adsorption and decomposition of perchloric acid (PA) on ZnO's most stable surfaces, *i.e.* {10–10} facets, were studied first. This is because PA is the key chain carrier in the decomposition of AP in its incipient stages, since PA is adsorbed on the surface of AP and prevents the continuous decomposition of AP.[30–32] In addition, catalysts such as ZnO have been introduced to promote the reaction of PA to boost the decomposition of AP. The exact computational details can be found in S-II and S-IV.† From Fig. S5,† the adsorption of a PA molecule on the ideal (10–10) surface is very weak and the calculated activation barrier for PA decomposition is as high as 1.98 eV, which implies that an ideal ZnO (10–10) surface is unlikely to contribute to the high catalytic performance. Moreover, there are no other exposed facets in T-ZnO from the above HRTEM characterization. Thus, the high reaction rate of PA decomposition on T-ZnO can be attributed to the observed step configurations. According to the HRTEM image in Fig. 2(c), a stick–ball model of the stepped configuration of a (10–10) surface along the [001] direction is shown in Fig. 3(a). Compared to the oxygen vacancy energy of around 3.72 eV in bulk ZnO,[33] the formation of an oxygen vacancy on a step edge is a relatively easy process with a thermodynamic barrier of around 0.5 eV. Such vacancies can be easily created through the abstraction of oxygen by NH_3 and other reductive species in the reaction process and are expected to be abundant along the step edges. Our calculation results show that the presence of a di-vacancy on the step edge could greatly enhance the adsorption energy as well as lower the reaction barrier. Once an oxygen di-vacancy is created on the step edges, we find that one of the O vacancy sites is energetically favorable for PA adsorption (Fig. 3(b)) and the binding energy is calculated to be −0.86 eV. Once adsorbed, the PA molecule would rotate along the [001] axis, with one of the O atoms in the PA molecule abstracted by the neighboring vacancy. The transition state will be encountered with two O atoms of PA residing in the two oxygen vacancies (Fig. 3(c)) and the energy barrier is 0.96 eV, much lower than that on an ideal (10–10) surface. Following the bond breaking of Cl–O, the final state of an active O^* and $HClO_3^*$ adsorbed on a stepped configuration is reached as shown in Fig. 3(d). The binding energy of the active O atom in the final state is calculated and its value would be 0.48 eV, indicating a higher reactivity in further redox

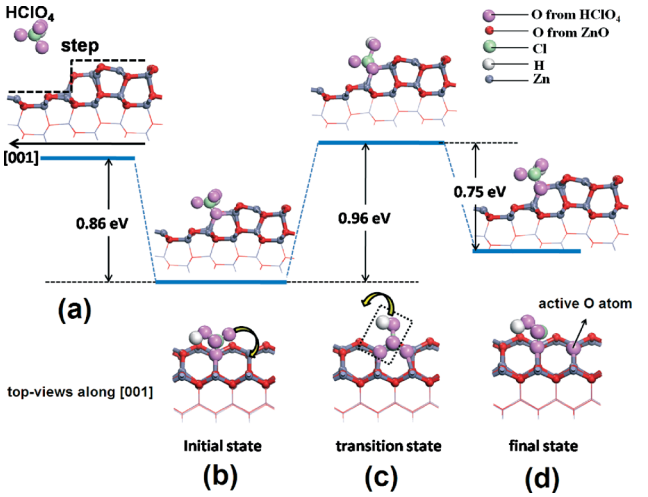

Fig. 3 A stick–ball model of decomposition of PA on the stepped structure of a ZnO (10–10) surface. (a) Step configurations along [001], (b) initial state of PA adsorbed on a stepped structure, (c) transition state of PA decomposition, and (d) final state of PA decomposition.

reactions. We thus conclude that the stepped structure of T-ZnO plays a crucial role in the high rate of PA decomposition.

Following the initiation stage, the oxidation exothermic reaction of NH_3 is a multistage process. Firstly, the adsorbed NH_3 can be activated to form NH intermediates through reaction of NH_3 with the formed active O atoms on the surface of T-ZnO. The oxidation reaction of NH occurs through the collision between NH and O adsorbed on the T-ZnO surface. Simultaneously, a series of reactions happen between gaseous NH and O on the surface of T-ZnO, and then the NH could interact with an oxygen atom (O) to form an HNO species, while two HNO species would interact to produce N_2O. The reaction pathways of the catalytic mechanism of T-ZnO nanoparticles are as described in eqn (1)–(4). This is similar to the proposed mechanism of selective catalytic oxidation of NH_3 to N_2 over Ag/Al_2O_3 by Zhang *et al.*,[34] in which the first step yields NH, and then the NH reacts with atomic oxygen (O) to form nitroxyl (HNO), which is further converted to N_2 or nitrous oxide (N_2O), or NH could even react with molecular O_2 to produce nitric oxide (NO); the *in situ*-formed NO interacts with the NH_x (x = 1, 2) and is reduced to N_2.

$$NH_3 + O \rightarrow NH + H_2O \quad (1)$$

$$NH + O \rightarrow HNO + H_2O \quad (2)$$

$$HNO + HNO \rightarrow N_2O + H_2O \quad (3)$$

$$N_2O + O \rightarrow NO \quad (4)$$

T-ZnO can return to its initial state after an active oxygen atom reacts with NH_x (x = 1–3). Therefore, T-ZnO should be considered as the catalyst accelerating both the diffusion of $HClO_4$ and the formation of active O atoms, which play a very important role in these chemical reactions. That is to say, T-ZnO have abundant atomic steps where the active O atoms

act as an active center during the decomposition of AP. As a result, the reverse reaction is held back, leading to the more complete oxidation reaction of ammonia. With an increase in the temperature, a series of reactions happen to gaseous NH_3 and NH with O on the T-ZnO surfaces, so the adsorbed layer of $HClO_4$ and NH_3 is decreased gradually. The oxidation of ammonia becomes more complete, and the activation energy of AP decomposition in HTD is decreased from 162.5 kJ mol^{-1} for pure AP to 111.9 kJ mol^{-1} for AP with T-ZnO as shown in Fig. 1.

The thermolysis process and its chemical reaction mechanism for pure AP and AP mixture with T-ZnO were systematically studied by means of an infrared spectra technique. Then, the real time species and their concentrations are obtained and identified by using rapid scanning Fourier transform infrared *in situ* spectroscopy. From Fig. 4, it can be seen that a set of bands are observed at ~2237, ~2204, ~1313 and ~1269 cm^{-1} which are associated with N_2O.[35] One band located at ~1630 and ~1590 cm^{-1} is assigned to NO. The other band located at ~2922 and ~2785 cm^{-1} is assigned to HCl. Also, the band located at ~3850, ~3736, ~3632, ~3563 and ~1690 cm^{-1} is assigned to H_2O(g). These results indicate that the main gaseous products of AP and a mixture of AP with T-ZnO are N_2O and NO. Additionally, small amounts of HCl and H_2O are produced from pure AP, which is similar to that in ref. 3. These results can also be considered as a confirmation for the schematic illustration of AP decomposition. The N_2O/NO intensity ratio is increased in LTD but is decreased in HTD when the test temperature is elevated for pure AP. This is because N_2O cannot be oxidized into NO continuously at LTD and the reverse reaction ($N_2O \rightarrow NH_3 \rightarrow NH_4ClO_4$) will occur, leading to the cessation of decomposition of pure AP. Interestingly, as the temperature rises, the values of N_2O/NO remain almost unchanged for the T-ZnO catalytic system all the time. It can be seen that T-ZnO will promote the oxidation of NH_3 and N_2O to produce NO species continuously, resulting in the decreased activation energy of AP decomposition. The experimental results are in good agreement with the theoretical calculations, further confirming that the atomic steps can facilitate the adsorption of $HClO_4$ and supply active oxygen atoms to react with NH_3, thus playing a key role in the decomposition of AP.

In summary, surface atomic steps of T-ZnO play very important roles in catalytic reaction, compared with well faceted R-ZnO. The findings of this work provide fundamental insight into the role of surface defects in catalytic activation and open up a novel strategy for significantly improving catalytic efficiency through controlling the surface defects of catalysts. We believe that the strategy may also be applied in the other catalysts, such as Fe_2O_3, CuO, *etc.*

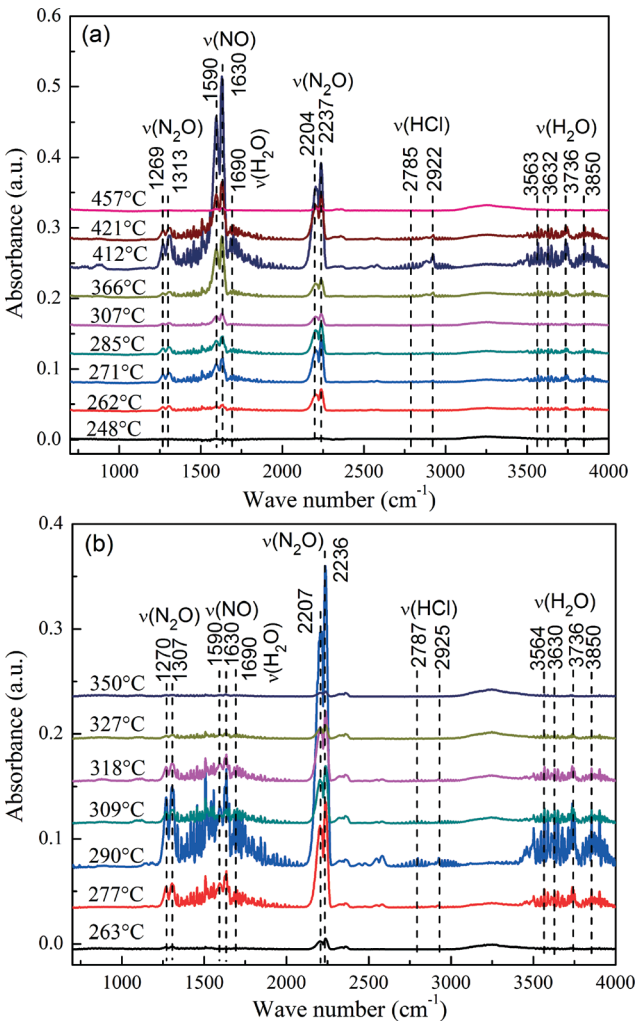

Fig. 4 IR spectra of decomposed gas products of pure AP (a) and mixtures of AP with T-ZnO (b) at different temperatures until they are completely decomposed.

Acknowledgements

This work was supported by the National Basic Research Program of China (grant no. 2009CB939702, 2013CB934800, and 2009CB939705) and Nature Science Foundation of China (no. 50772040 and 50927201). The technology was supported by the Analytic Testing Center of HUST, which is also acknowledged for its help in carrying out XRD and FESEM analyses. The authors acknowledge the Texas Advanced Computing Center (TACC) at The University of Texas at Austin (http://www.tacc.utexas.edu) for providing grid resources that have contributed to the research results reported within this paper.

Notes and references

1 L. L. Bircumshaw and B. H. Newman, *Proc. R. Soc. London, Ser. A*, 1955, **227**, 228.
2 J. N. Maycock and V. R. Pai Verneker, *Proc. R. Soc. London, Ser. A*, 1968, **307**, 303.
3 V. V. Boldyrev, *Thermochim. Acta*, 2006, **443**, 1.
4 V. V. Boldyrev, V. V. Alexandrov, A. V. Boldyreva, V. I. Gritsan, Yu. Ya. Karpenko, V. N. Korobeinitchev and E. F. Khairetdinov, *Combust. Flame*, 1970, **15**, 71.
5 P. W. M. Jacobs and W. L. Ng, *J. Phys. Chem. Solids*, 1972, **33**, 2031.
6 Y. P. Wang, J. W. Zhu, X. J. Yang, L. Lu and X. Wang, *Thermochim. Acta*, 2005, **437**, 106.

7 G. R. Duan, X. J. Yang, J. Chen, G. H. Huang, L. D. Lu and X. Wang, *Powder Technol.*, 2007, **172**, 27.
8 L. J. Chen, G. S. Li, P. Qi and L. P. Li, *J. Therm. Anal. Calorim.*, 2008, **92**, 765.
9 J. Wang, S. S. He, Z. S. Li, X. Y. Jing, M. L. Zhang and Z. H. Jiang, *Colloid Polym. Sci.*, 2009, **287**, 853.
10 H. Xu, X. B. Wang and L. Z. Zhang, *Powder Technol.*, 2008, **185**, 176.
11 L. P. Li, X. F. Sun, X. Q. Qiu, J. X. Xu and G. S. Li, *Inorg. Chem.*, 2008, **47**, 8839.
12 L. J. Chen, L. P. Li and G. S. Li, *J. Alloys Compd.*, 2008, **464**, 532.
13 G. Singh, I. P. S. Kapoor and S. Dubey, *Propellants, Explos., Pyrotech.*, 2009, **34**, 72.
14 D. V. Survase, M. Gupta and S. N. Asthana, *Prog. Cryst. Growth Charact. Mater.*, 2002, **45**, 161.
15 W. F. Chen, F. S. Li, L. L. Liu and Y. X. Li, *J. Rare Earths*, 2006, **24**, 782.
16 Z. X. Yu, Y. X. Sun, W. X. Wei, L. D. Lu and X. Wang, *J. Therm. Anal. Calorim.*, 2009, **97**, 903.
17 A. A. Said and R. A. Qasmi, *Thermochim. Acta*, 1996, **275**, 83.
18 T. Liu, L. S. Wang, P. Yang and B. Y. Hu, *Mater. Lett.*, 2008, **62**, 4056.
19 P. R. Patil, V. N. Krishnamurthy and S. S. Joshi, *Propellants, Explos., Pyrotech.*, 2008, **33**, 266.
20 Ü. Özgür, Y. I. Alivov, C. Liu, A. Teke, M. A. Reshchikov, S. Doğan, V. Avrutin, S. J. Cho and H. Morkoc, *J. Appl. Phys.*, 2005, **98**, 1.
21 X. F. Sun, X. Q. Qiu, L. P. Li and G. S. Li, *Inorg. Chem.*, 2008, **47**, 4146.
22 M. Zheng, Z. S. Wang, J. Q. Wu and Q. Wang, *J. Nanopart. Res.*, 2010, **12**, 2211.
23 J. Z. Yin, Q. Y. Lu, Z. N. Yu, J. J. Wang, H. Pang and F. Gao, *Cryst. Growth Des.*, 2010, **10**, 40.
24 F. Solymosi and L. Revesz, *Nature*, 1961, **192**, 64.
25 S. Q. Tian, D. W. Zeng, X. L. Peng, S. P. Zhang and C. S. Xie, *Sens. Actuators, B*, 2013, **181**, 509.
26 X. G. Han, H. Z. He, Q. Kuang, X. Zhou, X. H. Zhang, T. Xu, Z. X. Xie and L. S. Zheng, *J. Phys. Chem. C*, 2009, **113**, 584.
27 Z. Yang, L. M. Li and Q. Wan, *Sens. Actuators, B*, 2008, **135**, 57.
28 J. Song and S. Lim, *J. Phys. Chem. C*, 2007, **111**, 596.
29 B. Liu and H. C. Zeng, *J. Am. Chem. Soc.*, 2003, **125**, 4430.
30 P. W. M. Jacobs and A. R. Jones, *J. Phys. Chem.*, 1968, **72**, 202.
31 R. S. Zhu and M. C. Lin, *J. Phys. Chem. C*, 2008, **112**, 14481.
32 R. S. Zhu and M. C. Lin, *Comput. Theor. Chem.*, 2011, **965**, 328.
33 A. Janotti and C. G. Van de Walle, *Phys. Rev. B: Condens. Matter Mater. Phys.*, 2007, **76**, 1.
34 L. Zhang and H. He, *J. Catal.*, 2009, **268**, 18.
35 V. A. Matyshak and O. V. Krylov, *Catal. Today*, 1995, **25**, 1.

